

Nuclear shadowing and coherence length for longitudinal and transverse photons

Boris Kopeliovich,^{1,3} Jörg Raufeisen,^{1,2} and Alexander Tarasov^{1,3}

¹Max-Planck Institut für Kernphysik, Postfach 103980, D-69029 Heidelberg, Germany

²Institut für Theoretische Physik der Universität, Philosophenweg 19, D-69120 Heidelberg, Germany

³Joint Institute for Nuclear Research, Dubna, 141980 Moscow Region, Russia

(Received 15 March 2000; published 21 August 2000)

Motivated by the recent results for DIS off nuclei from the HERMES experiment we have performed a systematic study of shadowing for transverse and longitudinal photons. We found that the coherence length which controls the onset of nuclear shadowing at small x_{Bj} is much longer for longitudinal than transverse photons, and is much shorter for shadowing of gluons. The light-cone Green function approach we apply properly treats shadowing in the transition region $x_{Bj} > 0.01$. It also incorporates the nonperturbative effects and is legitimate at small Q^2 . We calculate nuclear shadowing and compare with data from the HERMES and NMC experiments. Although we expect different nuclear shadowing for longitudinal and transverse photons, numerically it cannot explain the strong effect observed by the HERMES Collaboration.

PACS number(s): 13.60.-r, 12.40.Vv, 25.30.Mr

I. INTRODUCTION

Recently the HERMES Collaboration released data [1] for shadowing in inclusive positron scattering off nuclei at medium high energies and Q^2 . The results expose few unusual features. The cross sections on nuclear targets, nitrogen, and helium-3, at small $x_{Bj} \approx 0.02$ and $Q^2 < 1 \text{ GeV}^2$ were found to be substantially more shadowed than one could expect extrapolating available data at higher Q^2 and energies. The observed enhancement of shadowing with Q^2 is also unusual. Interpreted in terms of different shadowing for transverse and longitudinal photons it was concluded in Ref. [1] that σ_L is enhanced, while σ_T is suppressed on nitrogen by at least a factor of two compared to deuteron target.

These data drew attention to the fact that very few data are available in this kinematical region. Moreover, no reliable theoretical calculations are done yet. The approach based on the nonlinear evolution equations [2,3] needs knowledge of the nuclear parton distribution at a medium-hard scale which is to be guessed, and is anyway outside the kinematical range we are interested in. More promising is the intuitive approach treating nuclear effects in the spirit of vector dominance model (VDM) [4] as shadowing for the total cross section of hadronic fluctuations of the virtual photon (see, e.g., Ref. [5]). However, the perturbative QCD treatment of the photon fluctuation can be applied only at high Q^2 , while VDM is sensible only at small $Q^2 \rightarrow 0$.

Progress was made recently [6] on the extension of perturbative QCD methods to the region of small Q^2 where the quarks in photon fluctuations cannot be treated as free. The nonperturbative interquark interaction was explicitly introduced and new light-cone $\bar{q}q$ wave functions were derived which recover the well-known perturbative ones at large Q^2 .

Nuclear shadowing is controlled by the interplay between two fundamental quantities. The lifetime of photon fluctuations, or coherence time is one. Namely, shadowing is possible only if the coherence time exceeds the mean inter-nucleon spacing in nuclei, and shadowing saturates (for a

given Fock component) if the coherence time substantially exceeds the nuclear radius.

Equally important for shadowing is the transverse separation of the $\bar{q}q$. In order to be shadowed the $\bar{q}q$ fluctuation of the photon has to interact with a large cross section. As a result of color transparency [7–9], small size dipoles interact only weakly and are therefore less shadowed. The dominant contribution to shadowing comes from the large aligned jet configurations [10,5] of the pair.

The mean lifetime of a $\bar{q}q$ fluctuation in vacuum calculated in Sec. II A turns out to be zero for transverse photons. This strange result is a consequence of an incorrect definition.

In Secs. II B and II C we propose a more sophisticated treatment of the coherence length or the fluctuation lifetime relevant for shadowing. The mean coherence time for the $\bar{q}q$ Fock state is evaluated using the perturbative and nonperturbative wave functions. The salient observation is that the coherence length is nearly three times longer for longitudinal than for transverse photons. At the same time, both are substantially different from the usual prescription $l_c = (2m_N x_{Bj})^{-1}$. The coherence length is found to vary steeply with Q^2 at fixed x_{Bj} and small Q^2 .

The coherence time for a $|\bar{q}qG\rangle$ Fock component controlling nuclear shadowing for gluons is calculated in Sec. II D. It turns out to be much shorter than for $|\bar{q}q\rangle$ components, therefore, the onset of gluon shadowing is expected at smaller x_{Bj} than for quarks.

The transition region between no shadowing at $x_{Bj} \sim 0.1$ and saturated (for the $|\bar{q}q\rangle$ component) shadowing at very small x_{Bj} is most difficult for theory. The impact parameter representation assigns definite cross sections to the fluctuations, but no definite mass which one needs to calculate the phase shift. On the other hand, the eigenstates of the mass matrix cannot be associated with any definite cross section. This controversy was settled within the light-cone Green function approach [11–13]. In Sec. III we rely on this approach to calculate nuclear shadowing in the kinematical re-

gion of the HERMES experiment. The nonperturbative light-cone wave functions and the realistic phenomenological dipole cross section are important at low Q^2 . We are unable to reproduce the data from the HERMES experiment, although our parameter-free calculations are in good agreement with NMC data. We do not expect any dramatic enhancement of the longitudinal cross section compared to the transverse one. At the same time, the calculated transverse cross section for nitrogen is shadowed by about 20% only, much less than the HERMES data need.

II. THE MEAN COHERENCE LENGTH

A. The lifetime for a perturbative $\bar{q}q$ fluctuation in vacuum

A photon of virtuality Q^2 and energy ν can develop a hadronic fluctuation for a lifetime

$$l_c = \frac{2\nu}{Q^2 + M^2} = \frac{P}{x_{Bj} m_N} = P l_c^{\max}, \quad (1)$$

where Bjorken $x_{Bj} = Q^2/2m_N\nu$, M is the effective mass of the fluctuation, factor $P = (1 + M^2/Q^2)^{-1}$, and $l_c^{\max} = 1/m_N x_{Bj}$. The usual approximation is to assume that $M^2 \approx Q^2$ since Q^2 is the only large dimensional scale available. In this case $P = 1/2$.

The effective mass of a noninteracting q and \bar{q} is well defined $M^2 = (m_q^2 + k_T^2)/\alpha(1-\alpha)$, where m_q and k_T and α are the mass, transverse momentum, and fraction of the light-cone momentum of the photon carried by the quark. Therefore, P has a simple form

$$P(k_T, \alpha) = \frac{Q^2 \alpha (1-\alpha)}{k_T^2 + \epsilon^2}, \quad (2)$$

where

$$\epsilon^2 = \alpha(1-\alpha)Q^2 + m_q^2. \quad (3)$$

To find the mean value of the fluctuation lifetime in vacuum one should average (2) over k_T and α weighted with the wave function squared of the fluctuation

$$\langle P \rangle_{\text{vac}} = \frac{\langle \Psi_{qq}^{\gamma^*} | P(k_T, \alpha) | \Psi_{qq}^{\gamma^*} \rangle}{\langle \Psi_{qq}^{\gamma^*} | \Psi_{qq}^{\gamma^*} \rangle}. \quad (4)$$

The perturbative distribution function for the $\bar{q}q$ has the form [14–16],

$$\Psi_{qq}^{T,L}(\vec{r}_T, \alpha) = \frac{\sqrt{\alpha_{em}}}{2\pi} \bar{\chi} \hat{O}^{T,L} \chi K_0(\epsilon r_T). \quad (5)$$

Here χ and $\bar{\chi}$ are the spinors of the quark and antiquark, respectively. $K_0(\epsilon r_T)$ is the modified Bessel function. The operators $\hat{O}^{T,L}$ have the form

$$\hat{O}^T = m_q \vec{\sigma} \cdot \vec{e} + i(1-2\alpha) (\vec{\sigma} \cdot \vec{n}) (\vec{e} \cdot \vec{\nabla}_T) + (\vec{\sigma} \times \vec{e}) \cdot \vec{\nabla}_T, \quad (6)$$

$$\hat{O}^L = 2Q\alpha(1-\alpha) \vec{\sigma} \cdot \vec{n}, \quad (7)$$

where the two-dimensional operator $\vec{\nabla}_T$ acts on the transverse coordinate \vec{r}_T ; $\vec{n} = \vec{p}/p$ is a unit vector parallel to the photon momentum; \vec{e} is the polarization vector of the photon.

The normalization integral in the denominator in the right-hand side of Eq. (4) diverges at large k_T for transversely polarized photons, therefore we arrive at the unexpected result $\langle P \rangle_{\text{vac}} = 0$.

B. Coherence length in nuclear medium

This puzzling conclusion can be interpreted as a result overwhelming the fluctuations of a transverse photon by heavy $\bar{q}q$ pairs with very large k_T . Such heavy fluctuations indeed have a very short lifetime. However, they also have a vanishing transverse size $r_T \sim 1/k_T$ and interaction cross section. Therefore, such fluctuations cannot be resolved by the interaction and do not contribute to the DIS cross section. To get a sensible result one should properly define the averaging procedure. We are interested in the fluctuations which contribute to nuclear shadowing, i.e., which interact at least twice. Correspondingly, the averaging procedure has to be redefined as

$$\langle P \rangle_{\text{shad}} = \frac{\langle f(\gamma^* \rightarrow \bar{q}q) | P(k_T, \alpha) | f(\gamma^* \rightarrow \bar{q}q) \rangle}{\langle f(\gamma^* \rightarrow \bar{q}q) | f(\gamma^* \rightarrow \bar{q}q) \rangle}, \quad (8)$$

where $f(\gamma^* \rightarrow \bar{q}q)$ is the amplitude of diffractive dissociation of the virtual photon on a nucleon $\gamma^* N \rightarrow \bar{q}q N$.

Thus, one should include in the weight the interaction cross section squared $\sigma_{qq}^2(r_T, s)$, where r_T is the transverse separation and $s = 2m_N\nu - Q^2 + m_N^2$. Then, the mean value of factor $P(\alpha, k_T)$ reads

$$\langle P^{T,L} \rangle = \frac{\int_0^1 d\alpha \int d^2r_1 d^2r_2 [\Psi_{qq}^{T,L}(\vec{r}_2, \alpha)]^* \sigma_{qq}^N(r_2, s) \bar{P}(\vec{r}_2 - \vec{r}_1, \alpha) \Psi_{qq}^{T,L}(\vec{r}_1, \alpha) \sigma_{qq}^N(r_1, s)}{\int_0^1 d\alpha \int d^2r |\Psi_{qq}^{T,L}(\vec{r}, \alpha) \sigma_{qq}^N(r, s)|^2} \quad (9)$$

with

$$\tilde{P}(\vec{r}_2 - \vec{r}_1, \alpha) = \int \frac{d^2 k_T}{(2\pi)^2} \exp[-i \vec{k}_T \cdot (\vec{r}_2 - \vec{r}_1)] P(\alpha, k_T). \quad (10)$$

Using expression (2) one obtains for a noninteracting $q\bar{q}$ pair,

$$\tilde{P}(\vec{r}_2 - \vec{r}_1, \alpha) = \frac{Q^2 \alpha (1 - \alpha)}{2\pi} K_0(\varepsilon |\vec{r}_2 - \vec{r}_1|). \quad (11)$$

As a simple estimate for the mean value (9) one can use the small- r_T approximation for the dipole cross section $\sigma_{q\bar{q}}^N(r_T, s) = C(s) r_T^2$. The factor $C(s)$ does not enter the result since it cancels in Eq. (9). We obtain for transverse and longitudinal photons

$$\langle P^T \rangle = \frac{2 Q^2}{3} \frac{\int_0^1 d\alpha (1 - \alpha) \alpha \left\{ [\alpha^2 + (1 - \alpha)^2] / \varepsilon^6 + \frac{7}{8} m_q^2 (1 - \alpha) \alpha / \varepsilon^8 \right\}}{\int_0^1 d\alpha \left\{ [\alpha^2 + (1 - \alpha)^2] / \varepsilon^4 + \frac{2}{3} m_q^2 / \varepsilon^6 \right\}}; \quad (12)$$

$$\langle P^L \rangle = \frac{7 Q^2}{8} \frac{\int_0^1 d\alpha (1 - \alpha)^3 \alpha^3 / \varepsilon^8}{\int_0^1 d\alpha (1 - \alpha)^2 \alpha^2 / \varepsilon^6}, \quad (13)$$

respectively.

We calculated the factor $\langle P^{T,L} \rangle$ as a function of Q^2 at $x_{Bj} = 0.01$ which is close to the minimal value in the HERMES data. We used the effective quark mass $m_q = 0.2$ GeV which corresponds to the confinement radius and allows us to reproduce data on nuclear shadowing [11]. Our results depicted in Fig. 1 by dotted lines are quite different from the naive estimate $P^{T,L} = 1/2$. In addition, P^L turns out to be substantially longer than P^T . This indicates that a longitudinally polarized photon develops lighter fluctuations than a transverse one. Indeed, the effective mass M is maximal for asymmetric pairs, i.e., when α or $1 - \alpha$ are small. However, such fluctuations are suppressed in longitudinal photons by the wave function (7).

The dependence of $\langle P^{T,L} \rangle$ on x_{Bj} depicted in Fig. 2 for $Q^2 = 4$ and 40 GeV is rather smooth. Therefore, the coherence length varies approximately as $l_c \propto 1/x_{Bj}$.

The simple approximation $\sigma_{q\bar{q}}^N \propto r_T^2$ is not realistic since nonperturbative effects affect the large- r_T behavior. Motivated by the phenomenon of confinement one should expect that gluons cannot propagate far away and the cross section should level off at large r_T . We use the modification [6] of the energy dependent phenomenological dipole cross section $\sigma_{q\bar{q}}^N(r_T, s)$ suggested in Ref. [17],

$$\sigma_{q\bar{q}}^N(r_T, s) = \sigma_0(s) \left[1 - \exp\left(-\frac{r_T^2}{r_0^2(s)}\right) \right], \quad (14)$$

where $r_0(s) = 0.88 (s/s_0)^{-0.14}$ fm, $s_0 = 1000$ GeV². This cross section is proportional to r_T^2 at small $r_T \rightarrow 0$, but is constant at large r_T . The energy dependence correlates with

r_T , at small r_T the dipole cross section rises steeper with energy than at large separations:

$$\sigma_0(s) = \sigma_{\text{tot}}^{\pi p}(s) \left(1 + \frac{3 r_0^2(s)}{8 \langle r_{ch}^2 \rangle_{\pi}} \right), \quad \langle r_{ch}^2 \rangle_{\pi} = 0.44 \text{ fm}^2, \quad (15)$$

where

$$\sigma_{\text{tot}}^{\pi p}(s) = 23.6 (s/s_0)^{0.08} \text{ mb}. \quad (16)$$

With this choice of $\sigma_{\text{tot}}^{\pi p}(s)$ one automatically reproduces the total cross section for pion proton scattering, while the parametrization from Ref. [17] cannot be applied to hadronic cross sections. Thus, cross section (14) is better designed for low and medium large $Q^2 < 10\text{--}20$ GeV², while at high Q^2 the parametrization [17] works better.

Equation (9) can be represented in the form

$$\langle P^{T,L} \rangle = \frac{N^{T,L}}{D^{T,L}}. \quad (17)$$

The angular integrations in Eq. (17) for the denominators $D^{T,L}$ are trivial and for the numerators $N^{T,L}$ one uses the relation [18]

$$K_0(\varepsilon |\vec{r}_1 - \vec{r}_2|) = K_0(\varepsilon r_>) I_0(\varepsilon r_<) + 2 \sum_{m=1}^{\infty} e^{im\phi} \times K_m(\varepsilon r_>) I_m(\varepsilon r_<), \quad (18)$$

where $r_> = \max(r_1, r_2)$, $r_< = \min(r_1, r_2)$, $\cos \phi = \vec{r}_1 \cdot \vec{r}_2 / (r_1 r_2)$, and $I_m(z)$ are the modified Bessel functions of first kind

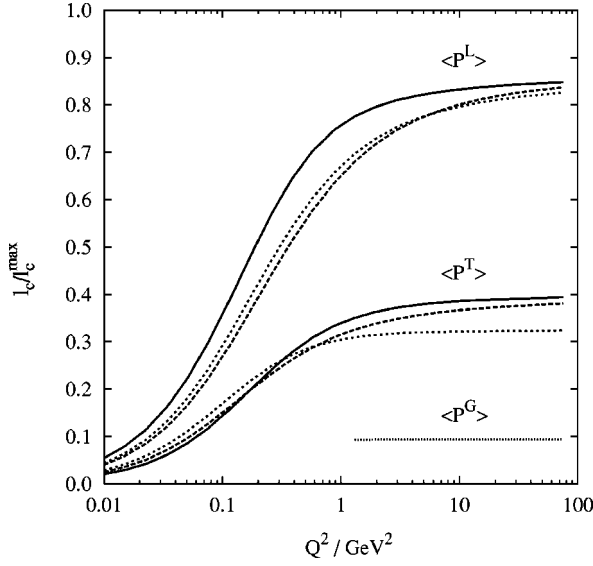


FIG. 1. Q^2 dependence of the factor $\langle P \rangle = l_c / l_c^{\max}$ defined in Eq. (1) at $x_{Bj} = 0.01$ for $\bar{q}q$ fluctuations of transverse and longitudinal photons, and for $\bar{q}qG$ fluctuation, from the top to bottom, respectively. Dotted curves correspond to calculations with perturbative wave functions and an approximate dipole cross section $\propto r_T^2$. Dashed curves are the same, except the realistic parametrization (14). The solid curves show the most realistic case based on the nonperturbative wave function (25). The coherence length for gluons calculated in Sec. II D is also shown.

(Bessel function of imaginary variable). It is clear from this relation that after angular integration only one term in the sum gives a nonvanishing contribution. We finally obtain for transverse photons

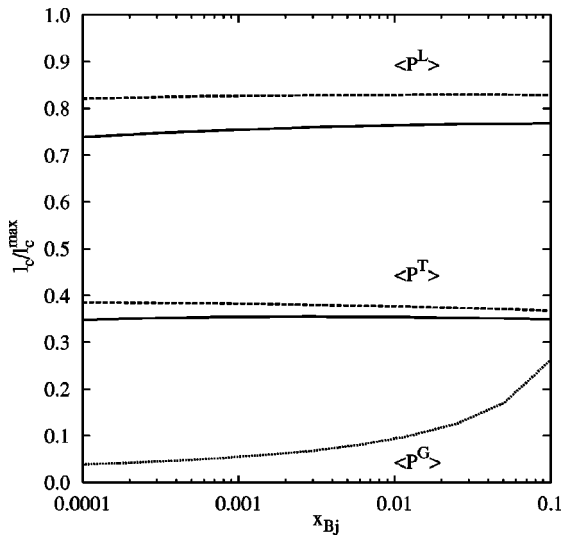


FIG. 2. x_{Bj} dependence of the factor $\langle P^{T,L} \rangle$ and $\langle P^G \rangle$ defined in Eq. (1) corresponding to the coherence length for shadowing of transverse and longitudinal photons and gluon shadowing, respectively. Solid and dashed curves correspond to $Q^2 = 4$ and 40 GeV^2 .

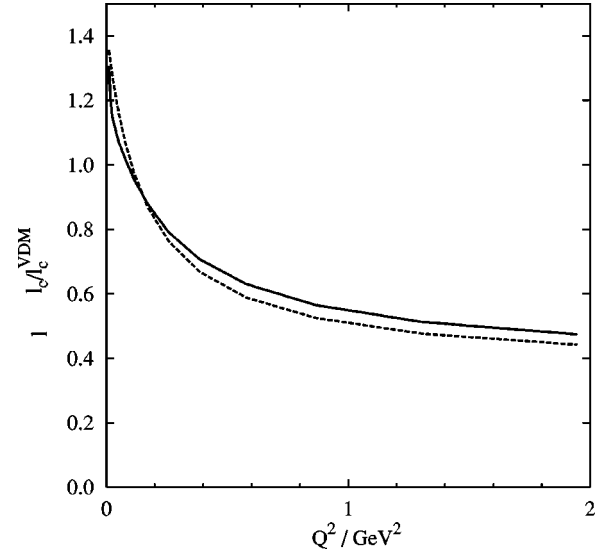


FIG. 3. Q^2 dependence of ratio of $\langle l_c^T \rangle$ calculated with Eq. (9) and $m_q = 200 \text{ MeV}$ to l_c^{VDM} calculated with Eq. (1) and $M = m_\rho$.

$$N_p^T = 2 Q^2 \int_0^1 d\alpha \alpha (1-\alpha) \int_0^\infty dr_2 r_2 \int_0^{r_2} dr_1 r_1 \{ m_q^2 K_0^2(\epsilon r_2) \times K_0(\epsilon r_1) I_0(\epsilon r_1) + [\alpha^2 + (1-\alpha)^2] \epsilon^2 K_1^2(\epsilon r_2) \times K_1(\epsilon r_1) I_1(\epsilon r_1) \} \sigma_{qq}^N(s, r_1) \sigma_{qq}^N(s, r_2), \quad (19)$$

$$D_p^T = \int_0^1 d\alpha \int_0^\infty dr r \{ m_q^2 K_0^2(\epsilon r) + [\alpha^2 + (1-\alpha)^2] \epsilon^2 K_1^2(\epsilon r) \} \times [\sigma_{qq}^N(s, r)]^2, \quad (20)$$

and for longitudinal photons

$$N_p^L = 2 Q^2 \int d\alpha \alpha^3 (1-\alpha)^3 \int_0^\infty dr_2 r_2 \int_0^{r_2} dr_1 r_1 K_0^2(\epsilon r_2) \times K_0(\epsilon r_1) I_0(\epsilon r_1) \sigma_{qq}^N(s, r_1) \sigma_{qq}^N(s, r_2), \quad (21)$$

$$D_p^L = \int d\alpha \int_0^\infty dr r \alpha^2 (1-\alpha)^2 K_0^2(\epsilon r) \sigma_{qq}^N(s, r)^2. \quad (22)$$

The factor $\langle P^{T,L}(x, Q^2) \rangle$ calculated in this way is depicted by dashed lines in Fig. 1 as a function of Q^2 at $x_{Bj} = 0.01$. It is not much different from the previous simplified estimate demonstrating low sensitivity to the form of the dipole cross section.

It is instructive to compare our predictions with the VDM which is usually supposed to dominate at small $Q^2 \ll m_\rho^2$. The corresponding coherence length l_c^{VDM} is given by Eq. (1) with $M = m_\rho$. The ratio of l_c^T calculated with the nonperturbative wave function to l_c^{VDM} as a function of Q^2 is shown by solid curve in Fig. 3. It demonstrates an unexpectedly precocious violation of VDM at quite low Q^2 . We also calculated l_c^T with the perturbative wave function, but with a massive

quark. With $m_q=200$ MeV it mimics the nonperturbative effects quite well, as one can see from Fig. 3.

C. Propagation of interacting $\bar{q}q$

Although the quarks should be treated perturbatively as nearly massless, at the end points α or $1-\alpha \rightarrow 0$ the mean $\bar{q}q$ transverse separation $r_T \sim 1/\epsilon$ becomes huge $\sim 1/m_q$. This contradicts the concept of confinement and should be regularized either by explicit introduction of a nonperturbative interaction between q and \bar{q} [6], or as is done below, introducing an effective quark mass.

Apparently, it is not legitimate to use the perturbative $\bar{q}q$ wave functions (5),(6) at low Q^2 where the nonperturbative interaction between q and \bar{q} becomes important. This interaction squeezes the $\bar{q}q$ wave packet, i.e., increases the intrinsic transverse momentum and the effective mass of the pair. By contributing to the effective mass of the $\bar{q}q$, the nonperturbative interaction breaks down the validity of the kinematical expression for M or Eq. (2). Even at high Q^2 at the end points α or $1-\alpha \rightarrow 0$ the mean $\bar{q}q$ transverse separation $r_T \sim 1/\epsilon$ becomes huge $\sim 1/m_q$ and nonperturbative corrections may be important. One can try to mimic these effects by an effective quark mass, as is done above, but one never knows how good this recipe is. To take the nonperturbative effects into account we use the light-cone Green function formalism suggested in [6] generalizing the perturbative description [11] of nuclear shadowing in DIS.

Propagation of an interacting $\bar{q}q$ pair in vacuum with initial separation \vec{r}_1 at the point with longitudinal coordinate z_1 up to point z_2 with final separation \vec{r}_2 is described by a Green function $G_{\bar{q}q}^-(\vec{r}_2, z_2; \vec{r}_1, z_1)$ which is a solution of a two-dimensional Schrödinger equation

$$\begin{aligned} & i \frac{d}{dz_2} G_{\bar{q}q}^{\text{vac}}(z_1, \vec{r}_1; z_2, \vec{r}_2) \\ &= \frac{\epsilon^2 - \Delta_{r_2} + a^4(\alpha) r_2^2}{2 \nu \alpha (1-\alpha)} G_{\bar{q}q}^{\text{vac}}(z_1, \vec{r}_1; z_2, \vec{r}_2). \end{aligned} \quad (23)$$

The nonperturbative oscillator potential contains function $a(\alpha) = a_0 + a_1 \alpha (1-\alpha)$ with parameters a_0 and a_1 fixed by data [6]. Data on total photoabsorption cross section, diffraction and nuclear shadowing are well described with

$$\begin{aligned} a^2(\alpha) &= v^{1.15} (112 \text{ MeV})^2 + (1-v)^{1.15} \\ &\times (165 \text{ MeV})^2 \alpha (1-\alpha), \end{aligned} \quad (24)$$

where v is any number satisfying $0 < v < 1$.

The Green function allows us to calculate the nonperturbative wave function for a $\bar{q}q$ fluctuation

$$\begin{aligned} \Psi_{\bar{q}q}^{T,L}(\vec{r}, \alpha) &= \frac{i Z_q \sqrt{\alpha_{em}}}{4 \pi p \alpha (1-\alpha)} \int_{-\infty}^{z_2} dz_1 (\bar{\chi} \hat{O}^{T,L} \chi) \\ &\times G_{\bar{q}q}^{\text{vac}}(z_1, \vec{r}_1; z_2, \vec{r}_2) \Big|_{r_1=0; \vec{r}_2=\vec{r}}. \end{aligned} \quad (25)$$

In the limit of vanishing interaction $a(\alpha) \rightarrow 0$ the wave functions (25) recovers the perturbative ones (5).

Note that in k_T representation the free Green function $G_{\bar{q}q}^0(z_1, \vec{r}_1; z_2, \vec{r}_2)$ integrated over longitudinal coordinate is simply related to the coherence length (1), if one performs an analytic continuation to imaginary time $z \rightarrow -iz$

$$\begin{aligned} & \int_{z_1}^{\infty} dz_2 G_{\bar{q}q}^0(z_1, \vec{r}_1; z_2, \vec{r}_2) \\ &= \int \frac{d^2 k_T}{(2\pi)^2} \exp[-i \vec{k}_T \cdot (\vec{r}_2 - \vec{r}_1)] l_c(k_T, \alpha). \end{aligned} \quad (26)$$

This is easily generalized to include the nonperturbative interaction. Then, making use of this relation one can switch in Eq. (9) to r_T representation and express the mean coherence length via the Green function. Then, we arrive at new expressions for the functions $N^{T,L}$ and $D^{T,L}$ in Eq. (17),

$$\begin{aligned} N^{T,L} &= \int_0^1 d\alpha \int d^2 r_1 d^2 r_2 [\Psi_{\bar{q}q}^{T,L}(\vec{r}_2, \alpha)]^* \sigma_{\bar{q}q}^N(r_2, s) \\ &\times \left(\int_{z_1}^{\infty} dz_2 G_{\bar{q}q}^{\text{vac}}(\vec{r}_1, z_1; \vec{r}_2, z_2) \right) \\ &\times \Psi_{\bar{q}q}^{T,L}(\vec{r}_1, \alpha) \sigma_{\bar{q}q}^N(r_1, s), \end{aligned} \quad (27)$$

$$D^{T,L} = \int_0^1 d\alpha \int d^2 r |\Psi_{\bar{q}q}^{T,L}(\vec{r}, \alpha) \sigma_{\bar{q}q}^N(r, s)|^2, \quad (28)$$

where the nonperturbative $\bar{q}q$ wave functions are given by Eq. (25).

For a harmonic oscillator potential the Green function is known analytically

$$\begin{aligned} G_{\bar{q}q}^{\text{vac}}(\vec{r}_2, z_1; \vec{r}_1, z_2) &= \frac{a^2(\alpha)}{2 \pi \sinh(\omega \Delta z)} \exp\left[-\frac{\epsilon^2 \Delta z}{2 \nu \alpha (1-\alpha)}\right] \\ &\times \exp\left\{-\frac{a^2(\alpha)}{2} \left[(r_1^2 + r_2^2) \coth(\omega \Delta z) \right. \right. \\ &\left. \left. - \frac{2 \vec{r}_1 \cdot \vec{r}_2}{\sinh(\omega \Delta z)} \right] \right\}, \end{aligned} \quad (29)$$

where $\Delta z = z_2 - z_1$ and

$$\omega = \frac{a(\alpha)^2}{\nu \alpha (1-\alpha)}, \quad (30)$$

is the oscillator frequency.

The light-cone wave functions (25) modified by the interaction can now be calculated explicitly [6]

$$\begin{aligned}
 & [\Psi_{q\bar{q}}^T(\varepsilon, \lambda, \vec{r}_1)]^* \Psi_{q\bar{q}}^T(\varepsilon, \lambda, \vec{r}_2) \\
 &= Z_q^2 \alpha_{em} [m_q^2 \Phi_0^*(\varepsilon, \lambda, \vec{r}_1) \Phi_0(\varepsilon, \lambda, \vec{r}_2) \\
 &+ [1 - 2\alpha(1 - \alpha)] \vec{\Phi}_1^*(\varepsilon, \lambda, \vec{r}_1) \cdot \vec{\Phi}_1(\varepsilon, \lambda, \vec{r}_2)], \tag{31}
 \end{aligned}$$

$$\begin{aligned}
 & [\Psi_{q\bar{q}}^L(\varepsilon, \lambda, \vec{r}_1)]^* \Psi_{q\bar{q}}^L(\varepsilon, \lambda, \vec{r}_2) \\
 &= Z_q^2 \alpha_{em} 4Q^2 \alpha^2 (1 - \alpha)^2 \Phi_0^*(\varepsilon, \lambda, \vec{r}_1) \Phi_0(\varepsilon, \lambda, \vec{r}_2), \tag{32}
 \end{aligned}$$

where the parameter

$$\lambda = \frac{2a^2(\alpha)}{\varepsilon^2}, \tag{33}$$

describes the strength of the interaction, and the functions $\Phi_{0,1}$ read

$$\begin{aligned}
 & \Phi_0^*(\varepsilon, \lambda, \vec{r}_1) \Phi_0(\varepsilon, \lambda, \vec{r}_2) \\
 &= \frac{1}{(4\pi)^2} \int_0^\infty du dt \frac{\lambda^2}{\sinh(\lambda t) \sinh(\lambda u)} \\
 &\times \exp\left[-\frac{\lambda \varepsilon^2 r_1^2}{4} \coth(\lambda t) - t - \frac{\lambda \varepsilon^2 r_2^2}{4} \coth(\lambda u) - u\right], \tag{34}
 \end{aligned}$$

$$\begin{aligned}
 & \vec{\Phi}_1^*(\varepsilon, \lambda, \vec{r}_1) \cdot \vec{\Phi}_1(\varepsilon, \lambda, \vec{r}_2) \\
 &= \frac{1}{(2\pi)^2} \frac{\vec{r}_1 \cdot \vec{r}_2}{r_1^2 r_2^2} \int_0^\infty du dt \\
 &\times \exp\left[-\frac{\lambda \varepsilon^2 r_1^2}{4} \coth(\lambda t) - t - \frac{\lambda \varepsilon^2 r_2^2}{4} \coth(\lambda u) - u\right]. \tag{35}
 \end{aligned}$$

It is easy to verify that in the limit of vanishing interaction, $\lambda \rightarrow 0$, the nonperturbative wave functions reduce to the perturbative ones. Compared to the expression for Φ_1 in Ref. [6], we have integrated by parts over the parameter u or t , respectively. This considerably simplifies the expression.

Now we have all ingredients which are necessary to calculate Eq. (17). Two from the eight remaining integrations, over the angles, can be performed analytically. We obtain

$$\begin{aligned}
 N^T &= m_N x_{Bj} \int_0^1 d\alpha \int_0^\infty dr_1 r_1 dr_2 r_2 \int_0^\infty d\Delta z [\Psi_{q\bar{q}}^T(\varepsilon, \lambda, \vec{r}_2)]^* \\
 &\times \Psi_{q\bar{q}}^T(\varepsilon, \lambda, \vec{r}_1) \sigma_{q\bar{q}}^N(r_2, s) \sigma_{q\bar{q}}^N(r_1, s) \frac{a^2(\alpha)}{\sinh(\omega \Delta z)} \\
 &\times \exp\left[-\frac{\varepsilon^2 \Delta z}{2\nu\alpha(1-\alpha)}\right] I_1\left[\frac{a^2(\alpha)r_1r_2}{\sinh(\omega \Delta z)}\right]
 \end{aligned}$$

$$\begin{aligned}
 & \times \exp\left[-\frac{a^2(\alpha)}{2}(r_1^2 + r_2^2) \coth(\omega \Delta z)\right], \tag{36} \\
 N^L &= m_N x_{Bj} \int_0^1 d\alpha \int_0^\infty dr_1 r_1 dr_2 r_2 \int_0^\infty d\Delta z [\Psi_{q\bar{q}}^L(\varepsilon, \lambda, \vec{r}_2)]^* \\
 &\times \Psi_{q\bar{q}}^L(\varepsilon, \lambda, \vec{r}_1) \sigma_{q\bar{q}}^N(r_2, s) \sigma_{q\bar{q}}^N(r_1, s) \frac{a^2(\alpha)}{\sinh(\omega \Delta z)}
 \end{aligned}$$

$$\begin{aligned}
 & \times \exp\left[-\frac{\varepsilon^2 \Delta z}{2\nu\alpha(1-\alpha)}\right] I_0\left[\frac{a^2(\alpha)r_1r_2}{\sinh(\omega \Delta z)}\right] \\
 & \times \exp\left[-\frac{a^2(\alpha)}{2}(r_1^2 + r_2^2) \coth(\omega \Delta z)\right], \tag{37}
 \end{aligned}$$

$$D^{L,T} = \int_0^1 d\alpha \int_0^\infty dr r |\Psi_{q\bar{q}}^{T,L}(\varepsilon, \lambda, \vec{r}) \sigma_{q\bar{q}}^N(r, s)|^2. \tag{38}$$

For a dipole cross section that levels off similar to Eq. (14) at large separations the integrations over r_1 and r_2 can also be done analytically. However, we prefer to work with the more general expressions that hold for arbitrary $\sigma_{q\bar{q}}^N(s, r)$, as long as it depends only on the modulus of r . We perform the remaining integrations numerically. The results for $I_c^{T,L}(x, Q^2)$ are shown by solid curves in Figs. 1 and 2.

D. Coherence length for gluon shadowing

Shadowing in the nuclear gluon distributing function at small x_{Bj} which looks similar to gluon fusion $GG \rightarrow G$ in the infinite momentum frame of the nucleus, should be treated in the rest frame of the nucleus as shadowing for the Fock components of the photon containing gluons. Indeed, the first shadowing term contains double scattering of the projectile gluon via exchange of two t -channel gluons, which is the same Feynman graph as gluon fusion. In addition, both correspond to the triple-Pomeron term in diffraction which controls shadowing.

The lowest gluonic Fock component is the $|\bar{q}qG\rangle$. The coherence length relevant to shadowing depends according to Eq. (1) on the effective mass of the $|\bar{q}qG\rangle$ which should be expected to be heavier than that for a $|\bar{q}q\rangle$, and even more for higher Fock components. Correspondingly, the coherence length $\langle l_c^G \rangle$ should be shorter and an onset of gluon shadowing is expected to start at smaller x_{Bj} .

For this coherence length one can use the same Eq. (1), but with the effective mass

$$M_{q\bar{q}G}^2 = \frac{k_T^2}{\alpha_G(1-\alpha_G)} + \frac{M_{q\bar{q}}^2}{1-\alpha_G}, \tag{39}$$

where α_G is the fraction of the photon momentum carried by the gluon, and $M_{q\bar{q}}^2$ is the effective mass of the $\bar{q}q$ pair. This formula is, however, valid only in the perturbative limit. It is apparently affected by the nonperturbative interaction of gluons which was found in Ref. [6] to be much stronger than that for a $\bar{q}q$. Since this interaction may substantially modify

the effective mass $M_{\bar{q}qG}^-$ we switch to the formalism of Green function described above, which recovers Eq. (39) in the limit of high Q^2 .

We treat gluons as massless and transverse. For factor P defined in Eq. (1) one can write

$$\langle P^G \rangle = \frac{N^G}{D^G}, \quad (40)$$

where

$$\begin{aligned} N^G &= m_N x_{Bj} \int d^2 r_{1G} d^2 r_{1q\bar{q}} d^2 r_{2G} d^2 r_{2q\bar{q}} d\alpha_q d \ln(\alpha_G) \\ &\times \tilde{\Psi}_{qqG}^\dagger(\vec{r}_{2G}, \vec{r}_{2q\bar{q}}, \alpha_q, \alpha_G) \\ &\times \left(\int_{z_1}^\infty dz_2 G_{\bar{q}qG}(\vec{r}_{2G}, \vec{r}_{2q\bar{q}}, z_2; \vec{r}_{1G}, \vec{r}_{1q\bar{q}}, z_1) \right) \\ &\times \tilde{\Psi}_{\bar{q}qG}(\vec{r}_{1G}, \vec{r}_{1q\bar{q}}, \alpha_q, \alpha_G), \quad (41) \\ D^G &= \int d^2 r_{1G} d^2 r_{1q\bar{q}} d^2 r_{2G} d^2 r_{2q\bar{q}} d\alpha_q d \ln(\alpha_G) \\ &\times \tilde{\Psi}_{qqG}^\dagger(\vec{r}_{2G}, \vec{r}_{2q\bar{q}}, \alpha_q, \alpha_G) \delta^{(2)}(\vec{r}_{2G} - \vec{r}_{1G}) \\ &\times \delta^{(2)}(\vec{r}_{2q\bar{q}} - \vec{r}_{1q\bar{q}}) \tilde{\Psi}_{\bar{q}qG}(\vec{r}_{1G}, \vec{r}_{1q\bar{q}}, \alpha_q, \alpha_G). \quad (42) \end{aligned}$$

Here we have introduced the Jacobi variables $\vec{r}_{q\bar{q}} = \vec{R}_q - \vec{R}_{\bar{q}}$ and $\vec{r}_G = \vec{R}_G - (\alpha_q \vec{R}_q + \alpha_{\bar{q}} \vec{R}_{\bar{q}}) / (\alpha_q + \alpha_{\bar{q}})$. $\vec{R}_{G,q,\bar{q}}$ are the position vectors of the gluon, the quark, and the antiquark in the transverse plane and $\alpha_{G,q,\bar{q}}$ are the longitudinal momentum fractions.

The Green function describing propagation of the $\bar{q}qG$ system satisfies the time evolution equation [6]

$$\begin{aligned} &\left[\frac{\partial}{\partial z_2} - \frac{Q^2}{2\nu} + \frac{\alpha_q + \alpha_{\bar{q}}}{2\nu\alpha_q\alpha_{\bar{q}}} \Delta_\perp(r_{q\bar{q}}) + \frac{\Delta_\perp(r_{2G})}{2\nu\alpha_G(1-\alpha_G)} \right. \\ &\quad \left. - V(\vec{r}_{2G}, \vec{r}_{2q\bar{q}}, \alpha_q, \alpha_G, z_2) \right] \\ &\times G_{\bar{q}qG}(\vec{r}_{2G}, \vec{r}_{2q\bar{q}}, z_2; \vec{r}_{1G}, \vec{r}_{1q\bar{q}}, z_1) \\ &= \delta(z_2 - z_1) \delta^{(2)}(\vec{r}_{2G} - \vec{r}_{1G}) \delta^{(2)}(\vec{r}_{2q\bar{q}} - \vec{r}_{1q\bar{q}}). \quad (43) \end{aligned}$$

In order to calculate the coherence length relevant to shadowing, we employ the amplitude for diffractive dissociation $\gamma^* \rightarrow \bar{q}qG$, which is the $\bar{q}qG$ wave function weighted by the cross section [6]

$$\begin{aligned} &\tilde{\Psi}_{\bar{q}qG}(\vec{r}_G, \vec{r}_{q\bar{q}}, \alpha_q, \alpha_G) \\ &= \Psi_{\bar{q}q}^{T,L}(\vec{r}_{q\bar{q}}, \alpha_q) \left[\Psi_{qG} \left(\frac{\alpha_G}{\alpha_q}, \vec{r}_G + \frac{\alpha_{\bar{q}}}{\alpha_q + \alpha_{\bar{q}}} \vec{r}_{q\bar{q}} \right) \right. \\ &\quad \left. - \Psi_{\bar{q}G} \left(\frac{\alpha_G}{\alpha_{\bar{q}}}, \vec{r}_G - \frac{\alpha_q}{\alpha_q + \alpha_{\bar{q}}} \vec{r}_{q\bar{q}} \right) \right] \\ &\times \frac{9}{8} \left[\sigma_{q\bar{q}}^N \left(s, \vec{r}_G + \frac{\alpha_{\bar{q}}}{\alpha_q + \alpha_{\bar{q}}} \vec{r}_{q\bar{q}} \right) \right. \\ &\quad \left. + \sigma_{q\bar{q}}^N \left(s, \vec{r}_G - \frac{\alpha_q}{\alpha_q + \alpha_{\bar{q}}} \vec{r}_{q\bar{q}} \right) - \sigma_{q\bar{q}}^N(s, r_{q\bar{q}}) \right]. \quad (44) \end{aligned}$$

As different from the case of the $|\bar{q}q\rangle$ Fock state, where perturbative QCD can be safely applied at high Q^2 , the non-perturbative effects remain important for the $|\bar{q}qG\rangle$ component even for highly virtual photons. High Q^2 squeezes the $\bar{q}q$ pair down to a size $\sim 1/Q$, however, the mean quark-gluon separation at $\alpha_G \ll 1$ depends on the strength of gluon interaction which is characterized in this limit by the parameter $b_0 \approx 0.65$ GeV [6]. For $Q^2 \gg b_0^2$ the $\bar{q}q$ is small, $r_{\bar{q}q}^2 \ll r_G^2$, and one can treat the $\bar{q}qG$ system as a color octet-dipole, i.e.,

$$\begin{aligned} &G_{\bar{q}qG}(\vec{r}_{2G}, \vec{r}_{2q\bar{q}}, z_2; \vec{r}_{1G}, \vec{r}_{1q\bar{q}}, z_1) \\ &\Rightarrow G_{q\bar{q}}(\vec{r}_{2q\bar{q}}, z_2; \vec{r}_{1q\bar{q}}, z_1) G_{GG}(\vec{r}_{2G}, z_2; \vec{r}_{1G}, z_1). \quad (45) \end{aligned}$$

Such a Green function G_{GG} satisfies the simple evolution equation [6]

$$\begin{aligned} &\left[\frac{\partial}{\partial z_2} - \frac{Q^2}{2\nu} + \frac{\Delta_\perp(r_{2G})}{2\nu\alpha_G(1-\alpha_G)} - \frac{b_0^4 r_{2G}^2}{2\nu\alpha_G(1-\alpha_G)} \right] \\ &\times G_{GG}(\vec{r}_{2G}, z_2; \vec{r}_{1G}, z_1) \\ &= \delta(z_2 - z_1) \delta^{(2)}(\vec{r}_{2G} - \vec{r}_{1G}). \quad (46) \end{aligned}$$

Correspondingly, the modified $\bar{q}qG$ wave function simplifies too,

$$\begin{aligned} &\tilde{\Psi}_{\bar{q}qG}(\vec{r}_G, \vec{r}_{q\bar{q}}, \alpha_q, \alpha_G) \\ &\Rightarrow -\Psi_{q\bar{q}}^L(\vec{r}_{q\bar{q}}, \alpha_q) \vec{r}_{q\bar{q}} \cdot \vec{\nabla} \Psi_{qG}(\vec{r}_G) \sigma_{GG}^N(s, r_G), \quad (47) \end{aligned}$$

where the nonperturbative quark-gluon wave function has the form [6]

$$\begin{aligned}\Psi_{qG}(\vec{r}_G) &= \lim_{\alpha_G \rightarrow 0} \Psi_{qG}(\alpha_G, r_G) \\ &= -\frac{2i}{\pi} \sqrt{\frac{\alpha_s}{3}} \frac{\vec{e} \cdot \vec{r}_G}{r_G^2} \exp\left(-\frac{b_0^2}{2} r_G^2\right),\end{aligned}\quad (48)$$

and the color-octet dipole cross section reads

$$\sigma_{GG}^N(s, r_G) = \frac{9}{4} \sigma_{qq}^N(s, r_G). \quad (49)$$

With the approximations given above, the factor $\langle P^G \rangle$ in Eq. (1) for the gluon coherence length is calculated in the Appendix and has the form

$$\begin{aligned}\langle P^G \rangle &= \frac{2}{3 \ln(\alpha_G^{\max}/\alpha_G^{\min})} \int_{\delta^{\min}}^{\delta^{\max}} \frac{d\delta}{\delta} \left\{ \frac{5}{8(1+\delta)} + \frac{7}{8(1+3\delta)} \right. \\ &\quad \left. - \frac{\delta}{\delta^2-1} \left[\psi(2) - \psi\left(\frac{3}{2} + \frac{1}{2\delta}\right) \right] \right\},\end{aligned}\quad (50)$$

where

$$\psi(x) = \frac{d \ln \Gamma(x)}{dx}, \quad \delta = \frac{2b_0^2}{Q^2 \alpha_G}. \quad (51)$$

Both the numerator and denominator in Eq. (50) diverge logarithmically for $\alpha_G^{\min} \rightarrow 0$, as it is characteristic for radiation of vector bosons. To find an appropriate lower cutoff, note that the mass of the $q\bar{q}G$ system is approximately given by

$$M_{q\bar{q}G}^2 \approx \frac{2b_0^2}{\alpha_G} + Q^2, \quad (52)$$

where we used Eq. (39) with $\langle k_T^2 \rangle \approx b_0^2$. We demand that $M_{q\bar{q}G}^2 < 0.2s$ which leads to $\alpha_G^{\min} = 2b_0^2/(0.2s - Q^2)$. Furthermore we work in the approximation of $\alpha_G \ll 1$ and we also have to choose an upper cutoff. We use

$$\frac{2b_0^2}{0.2s - Q^2} \leq \alpha_G \leq \frac{2b_0^2}{Q^2}, \quad (53)$$

which means that we take only masses $2Q^2 \leq M_{q\bar{q}G}^2 \leq 0.2s$ into account. The two limits become equal at $x_{Bj} \approx 0.1$.

Our results for $\langle P^G \rangle = \langle l_c^G \rangle / l_c^{\max}$ are depicted in Fig. 1. With approximations made above we cannot cover the low Q^2 region and perform calculations at $Q^2 > 1 \text{ GeV}^2$. The found coherence length is much shorter than both l_c^T and l_c^L for $|q\bar{q}\rangle$ fluctuations. This conclusion corresponds to a delayed onset of gluon shadowing shifted to smaller x_{Bj} predicted in Ref. [6].

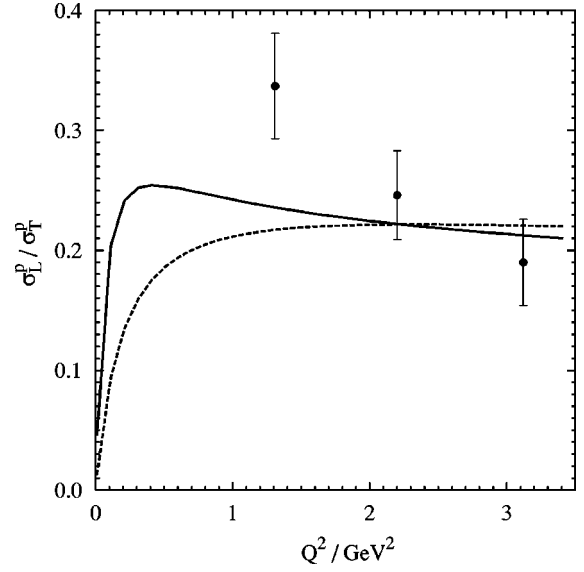


FIG. 4. Ratio of longitudinal to transverse photoabsorption cross sections as a function of Q^2 at $x_{Bj}=0.01$. The solid curve is calculated with Eq. (54) and the wave functions including the nonperturbative effects, while for the dashed curve the perturbative wave functions with $m_q=200 \text{ MeV}$ are used. The NMC data points [19] correspond to $x_{Bj}=0.008, 0.0125, 0.0175$ from smaller to higher Q^2 .

III. SHADOWING FOR LONGITUDINAL AND TRANSVERSE PHOTONS

A. σ_L/σ_T on a nucleon target

As soon as realistic wave functions for $\bar{q}q$ fluctuations including the nonperturbative effects are available, as well as the energy dependent phenomenological dipole cross section, we are in position to calculate the longitudinal and transverse cross sections for a proton target covering also the region of small Q^2 ,

$$\sigma_{T,L}^{\gamma^*p} = \int_0^1 d\alpha \int d^2r |\Psi_{q\bar{q}}^{T,L}(\vec{r}, \alpha)|^2 \sigma_{qq}^N(r, s). \quad (54)$$

The results of calculations for the ratio σ_L/σ_T is shown in Fig. 4 by solid curve as a function of Q^2 at $x_{Bj}=0.01$ which is about the lowest value of x_{Bj} in the HERMES data. As one could expect the ratio vanishes towards $Q^2=0$, however, it is nearly constant down to very small $Q^2 \approx 0.3 \text{ GeV}^2$. To see how well an effective quark mass can mimic the effect of the nonperturbative interactions we have also performed calculations with the perturbative wave functions and $m_q=200 \text{ MeV}$ and plotted the results by dashed curve in Fig. 4. Comparison demonstrates a substantial difference at small Q^2 .

B. Nuclear targets

Although the coherence length is an important characteristic for shadowing, it is not sufficient to predict nuclear effects in the structure function. Shadowing for parton densities at small x_{Bj} in the nuclear structure function which is defined in the infinite momentum frame originates from the

nonlinear effect of parton fusion in the evolution equation [2,3]. Although the partonic treatment varies from one to another reference frame, all observables including shadowing are Lorentz invariant. In the rest frame of the nucleus shadowing in the total virtual photoabsorption cross section $\sigma_{\text{tot}}^{\gamma^*A}$ (or the structure function F_2^A) can be decomposed over different Fock components of the photon

$$\begin{aligned} \sigma_{\text{tot}}^{\gamma^*A} = & A \sigma_{\text{tot}}^{\gamma^*N} - \Delta \sigma_{\text{tot}}(\bar{q}q) - \Delta \sigma_{\text{tot}}(\bar{q}qG) \\ & - \Delta \sigma_{\text{tot}}(\bar{q}q2G) - \dots \end{aligned} \quad (55)$$

According to above calculations and Fig. 4 the coherence length corresponding to gluon shadowing is rather small compared to the mean internucleon spacing in a nucleus in the kinematical region we are interested in. Therefore, we hold only the first two terms in the right-hand side of Eq. (55), which can be represented for transverse and longitudinal photons as

$$\begin{aligned} (\sigma_{\text{tot}}^{\gamma^*A})^{T,L} = & A (\sigma_{\text{tot}}^{\gamma^*N})^{T,L} \\ & - \frac{1}{2} \text{Re} \int d^2b \int_0^1 d\alpha \int_{-\infty}^{\infty} dz_1 \int_{z_1}^{\infty} dz_2 \int d^2r_1 \\ & \times \int d^2r_2 [\Psi_{qq}^{T,L}(\varepsilon, \lambda, r_2)]^* \rho_A(b, z_2) \sigma_{qq}^N(s, r_2) \\ & \times G(\vec{r}_2, z_2 | \vec{r}_1, z_1) \rho_A(b, z_1) \\ & \times \sigma_{qq}^N(s, r_1) \Psi_{qq}^{T,L}(\varepsilon, \lambda, r_1), \end{aligned} \quad (56)$$

where $\rho_A(b, z)$ is the nuclear density dependent on impact parameter b and longitudinal coordinate z . The nonperturbative wave functions for the $\bar{q}q$ component of the photon are defined in Eqs. (31),(32). The Green function $G(\vec{r}_2, z_2 | \vec{r}_1, z_1)$ describes propagation of a nonperturbatively interacting $\bar{q}q$ pair in an absorptive medium. It fulfills the evolution equation

$$\begin{aligned} \left[i \frac{\partial}{\partial z_2} + \frac{\Delta_{\perp}(r_2) - \varepsilon^2}{2\nu\alpha(1-\alpha)} + \frac{i}{2} \rho_A(b, z_2) \sigma_{qq}^N(s, r_2) \right. \\ \left. - \frac{a^4(\alpha)r_2^2}{2\nu\alpha(1-\alpha)} \right] G(\vec{r}_2, z_2 | \vec{r}_1, z_1) \\ = i \delta(z_2 - z_1) \delta^{(2)}(\vec{r}_2 - \vec{r}_1), \end{aligned} \quad (57)$$

where $a(\alpha)$ and λ were introduced in Eqs. (24) and (33), respectively. The third term in the left-hand side of Eq. (57) describes absorption of the $\bar{q}q$ pair in the medium of density $\rho_A(b, z)$ with cross section $\sigma_{qq}^N(s, r)$. At small x_{Bj} when the coherence length substantially exceeds, $l_c^{T,L} \gg (z_2 - z_1)$ (the nuclear radius) the solution of Eq. (57) very much simplifies, $G(\vec{r}_2, z_2 | \vec{r}_1, z_1) \propto \delta^{(2)}(\vec{r}_2 - \vec{r}_1)$, i.e., Lorentz time dilation ‘‘freezes’’ variation of transverse $\bar{q}q$ separation.

Correspondingly, the total cross section gets a simple form [7,16]

$$\begin{aligned} (\sigma_{\text{tot}}^{\gamma^*A})_{\nu \rightarrow \infty}^{T,L} = & 2 \int d\alpha \int d^2r |\Psi_{qq}^{T,L}(\varepsilon r)|^2 \\ & \times \int d^2b \left[1 - \exp\left(-\frac{\sigma_{qq}^N(r)}{2} T(b)\right) \right], \end{aligned} \quad (58)$$

where

$$T(b) = \int_{-\infty}^{\infty} dz \rho_A(b, z) \quad (59)$$

is the thickness function of the nucleus. Equation (57) has an explicit analytical solution only if the dipole cross section $\sigma_{qq}^N(r) = C r^2$ and the nuclear density is constant $\rho_A(b, z) = \rho_0$. Such an approximation has a reasonable accuracy, especially for heavy nuclei. Nevertheless, it can be even more precise if one makes use of the fact that the asymptotic expression (58) is easily calculated with exact (realistic) dipole cross section and nuclear density. We need to use the solution of Eq. (57) only in the transition region from no-shadowing to a fully developed shadowing given by Eq. (58). First of all, we fixed factor C in the simplified dipole cross section demanding to have the same asymptotic shadowing Eq. (58) as with the realistic one given by Eq. (14). This was done with the realistic Woods-Saxon form for nuclear density [20] and separately for transverse and longitudinal photons and for each value of α . Then we switched to a constant nuclear density ρ_0 , demanding it to lead to the same asymptotic shadowing in Eq. (58) as with the realistic one. We have checked that the found value of ρ_0 is practically independent of the value of the cross section in the interval 1–50 mb.

First of all we have checked our formalism comparing with the NMC results for shadowing in the nuclear structure function. Figure 5 demonstrates the data [21] for tin to carbon ratio of proton structure functions depicted by full circles. As was pointed out above gluon shadowing is negligibly small at $x_{Bj} > 0.01$ which covers the whole range on the NMC experiment. We performed calculations with parameter $\nu = 0.5$ in Eq. (24), but we have checked that the results are independent of ν . Although the calculations are parameter free, agreement is pretty good.

Eventually, we are able to provide predictions for the kinematical range of HERMES. The ratio of the virtual photoabsorption cross sections for nitrogen to hydrogen at $x_{Bj} = 0.01$ versus Q^2 is plotted in Fig. 6. The solid and dashed curves correspond to the nonperturbative and perturbative wave functions, respectively. A salient feature of these predictions is shadowing vanishing towards $Q^2 = 0$. This observation does not contradict the well known fact of shadowing for real photo absorption, but is a rather simple consequence of kinematics. The colliding energy $s = Q^2 x_{Bj}$ vanishes along with Q^2 at fixed x_{Bj} . This example shows that x_{Bj} is a poor variable at small Q^2 and should be replaced by s . This kinematical effect may be partially responsible for the unusual enhancement of nuclear shadowing with rising Q^2 detected in the HERMES experiment [1]. Our calculated nitro-

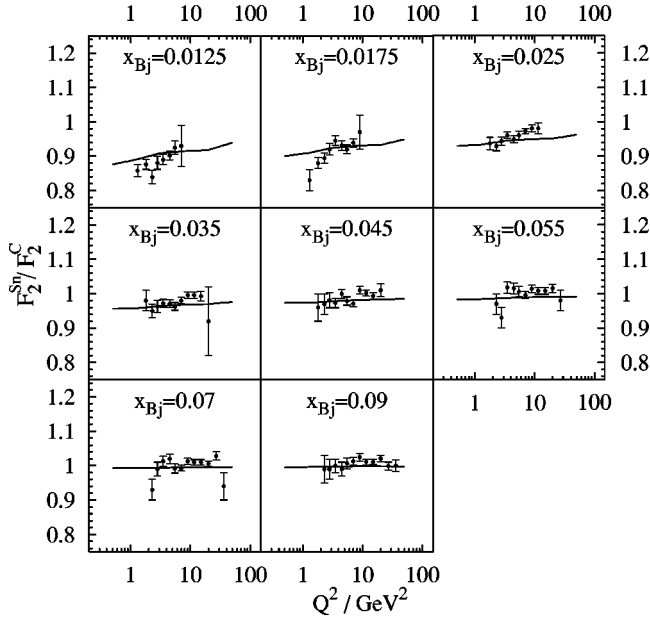


FIG. 5. Q^2 and x_{Bj} dependence of structure function ratio for tin to carbon. Full circles show the NMC data [21]. The crosses show the results of our calculations for the same kinematics.

gen to proton ratio of the cross sections reaches its minimum at $Q^2 \sim 0.2$ GeV² and then smoothly rises with Q^2 .

The most striking feature of the HERMES data for shadowing is a dramatically rising $R = \sigma_L/\sigma_T$ ratio on nitrogen compared to proton target at $Q^2 < 1$ GeV² [1]. Our predictions for R_N/R_p are plotted in Fig. 7 versus Q^2 at $x_{Bj} = 0.01$ where the experimental ratio $R_N/R_p \approx 5$. Apparently, we do not expect any remarkable effect. Moreover, this ratio does not change much from proton to nitrogen in spite of the much longer coherence length for longitudinal photons predicted above. However, this effect leading to a stronger shadowing for σ_L is compensated by the fact that longitudinal

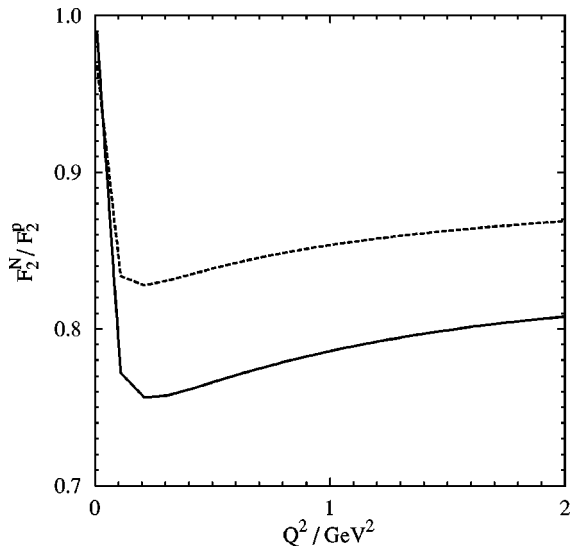


FIG. 6. The shadowing ratio for nitrogen over proton at low Q^2 and $x_{Bj} = 0.01$. Shadowing disappears as $Q^2 \rightarrow 0$, because of the vanishing coherence length.

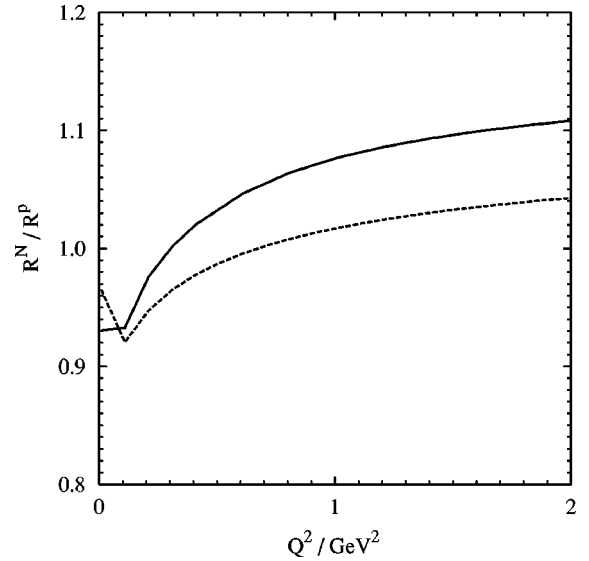


FIG. 7. Ratio of longitudinal to transverse fractions of the cross section $R = \sigma_L/\sigma_T$ on nitrogen to proton targets. The solid and dashed curves correspond to the photon wave function with and without nonperturbative effects.

photons develop fluctuations of a smaller size compared to that in transverse photons, i.e., they are less shadowed. Note that nuclear effects for R were estimated previously in Ref. [22] where many of the important ingredients of present approach were missed.

IV. SUMMARY

Based on the light-cone Green function approach we provide predictions for nuclear shadowing in the most difficult for calculation region of medium-small $x_{Bj} > 0.01$. Since the nonperturbative effects are included we also predict shadowing down to small $Q^2 < 1$ GeV² which is the kinematical region where the HERMES experiment discovered unusual shadowing effects.

We found that the coherence length which controls shadowing is nearly three times longer for longitudinal than for transverse photons, and it is very much different from what is suggested by the widely accepted approximation. Using the Green-function light-cone approach including the nonperturbative effects we calculated nuclear shadowing for longitudinal and transverse photons. Although the predicted nuclear shadowing exposes interesting effects in the region of small Q^2 , we are unable to explain the dramatic phenomena detected in the HERMES experiment.

We suppose that our results provide a reliable base line for nuclear effects in this region. The dramatic effects revealed by the HERMES experiment probably cannot be explained without involving a new nonstandard dynamics (e.g., see Ref. [23]).

ACKNOWLEDGMENTS

We are grateful to Andreas Schäfer who initiated this work and actively participated in it during the early stages, for numerous and encouraging discussions. We thank Antje

Brüll, Jeroen van Hunen, and Gerard van der Steenhoven for informing us about the unusual observation in the HERMES experiment and for many helpful communications and discussions. We are also thankful to Yuri Ivanov for help with preparing figures. This work was partially supported by the Gesellschaft für Schwerionenforschung, GSI, Grant No. HD HÜF T, by Grant No. INTAS-97-OPEN-31696, and by the European Network: Hadronic Physics with Electromagnetic Probes, Contract No. FMRX-CT96-0008. Most of this work was done when A.V.T. was employed by Regensburg University. J.R. was partially supported by the Gradviertenkolleg ‘‘Physikalische Systeme mit vielen Freiheitsgraden.’’

APPENDIX: CALCULATION OF THE COHERENCE LENGTH FOR THE $\bar{q}qG$ STATE

The calculations are somewhat more cumbersome for the gluon coherence length. We consider the case $Q^2 \gg b_0^2$. With the approximations (45)–(47) we obtain for the denominator of Eq. (40)

$$D^G = \int d^2r_G d^2r_{q\bar{q}} \int_0^1 d\alpha_q \int_{\alpha_G^{\min}}^{\alpha_G^{\max}} \frac{d\alpha_G}{\alpha_G} |\Psi^L(r_{q\bar{q}}\alpha_{q\bar{q}})|^2 \times [\sigma_{q\bar{q}}^N(s, r_G)]^2 [\vec{r}_{q\bar{q}} \cdot \vec{\nabla} \Psi_{qG}(r_G)]^2. \quad (\text{A1})$$

This integral diverges logarithmically for $\alpha_G^{\min} \rightarrow 0$. To find an appropriate lower cutoff, note that the mass of the $q\bar{q}G$ system is approximately given by

$$M_{q\bar{q}G}^2 \approx \frac{2b_0^2}{\alpha_G} + Q^2. \quad (\text{A2})$$

We demand that $M_{q\bar{q}G}^2 < 0.2s$ which leads to $\alpha_G^{\min} = 2b_0^2/(0.2s - Q^2)$. Furthermore we work in the approximation of $\alpha_G \ll 1$ and we also have to choose an upper cutoff. We use

$$\frac{2b_0^2}{0.2s - Q^2} \leq \alpha_G \leq \frac{2b_0^2}{Q^2}. \quad (\text{A3})$$

The two limits become equal at $x_{Bj} \approx 0.1$. In our further calculation of D^G we do the replacement $r_{q\bar{q}i} r_{q\bar{q}j} \rightarrow r_{q\bar{q}}^2 \delta_{ij}$ and perform the derivative. This yields

$$D^G = \left(\frac{2}{\pi} \sqrt{\frac{\alpha_s}{3}} \right)^2 \frac{6\alpha_{em}}{(2\pi)^2} 4Q^2 \pi \int d^2r_G d^2r_{q\bar{q}} r_{q\bar{q}}^3 \times \int_0^1 d\alpha_q \int_{\alpha_G^{\min}}^{\alpha_G^{\max}} \frac{d\alpha_G}{\alpha_G} K_0^2(\epsilon r_{q\bar{q}}) \alpha_q^2 (1 - \alpha_q)^2 \times [\sigma_{q\bar{q}}^N(s, r_G)]^2 e^{-b_0^2 r_G^2} \left(\frac{2}{r_G^4} + \frac{2b_0^2}{r_G^2} + b_0^4 \right). \quad (\text{A4})$$

For the integration over $r_{q\bar{q}}$ we use the integral representation

$$K_0(x) = \frac{1}{2} \int_0^\infty \frac{dt}{t} \exp\left(-t - \frac{x^2}{4t}\right) \quad (\text{A5})$$

of the modified Bessel function and obtain

$$\int_0^\infty dr_{q\bar{q}} r_{q\bar{q}}^3 K_0^2(\epsilon r_{q\bar{q}}) = \frac{2}{3\epsilon^4}. \quad (\text{A6})$$

Thus we have for the denominator

$$D^G = \frac{32\alpha_{em}\alpha_s}{3\pi^2 Q^2} \ln \frac{\alpha_G^{\max}}{\alpha_G^{\min}} \int_0^\infty dr_G r_G [\sigma_{q\bar{q}}^N(s, r_G)]^2 \times e^{-b_0^2 r_G^2} \left(\frac{2}{r_G^4} + \frac{2b_0^2}{r_G^2} + b_0^4 \right). \quad (\text{A7})$$

Now we restrict ourselves to the dipole cross section of the form

$$\sigma_{q\bar{q}}^N(s, r_G) = C(s) r_G^2 \quad (\text{A8})$$

and perform the last integration with the result

$$D^G = \frac{32\alpha_{em}\alpha_s C^2(s)}{\pi^2 Q^2 b_0^2} \ln \frac{\alpha_G^{\max}}{\alpha_G^{\min}}. \quad (\text{A9})$$

Note that the factor $C(s)$ will drop out, when one takes the ratio $\langle P^G \rangle = N^G/D^G$.

Next we calculate the numerator

$$N^G = m_N x_{Bj} \left(\frac{2}{\pi} \sqrt{\frac{\alpha_s}{3}} \right)^2 \frac{6\alpha_{em}}{(2\pi)^2} 4Q^2 \int d^2r_{1G} d^2r_{2G} d^2r_{q\bar{q}} \times \int_0^1 d\alpha_q \int_{\alpha_G^{\min}}^{\alpha_G^{\max}} \frac{d\alpha_G}{\alpha_G} \alpha_q^2 (1 - \alpha_q)^2 \times K_0^2(\epsilon r_{q\bar{q}}) \sigma_{q\bar{q}}^N(s, r_{1G}) \sigma_{q\bar{q}}^N(s, r_{2G}) \times \left[\vec{r}_{q\bar{q}} \cdot \vec{\nabla}_{r_{1G}} \frac{\vec{e} \cdot \vec{r}_{1G}}{r_{1G}^2} e^{-b_0^2 r_{1G}^2/2} \right] \times \left[\vec{r}_{q\bar{q}} \cdot \vec{\nabla}_{r_{2G}} \frac{\vec{e} \cdot \vec{r}_{2G}}{r_{2G}^2} e^{-b_0^2 r_{2G}^2/2} \right] \times \int_0^\infty d\Delta z G_{GG}(\vec{r}_{2G}, \vec{r}_{1G}, \Delta z), \quad (\text{A10})$$

where

$$G_{GG}(\vec{r}_{2G}, \vec{r}_{1G}, \Delta z) = \frac{b_0^2 e^{Q^2 \Delta z/2\nu}}{2\pi \sinh(\omega \Delta z)} \exp\left\{ -\frac{b_0^2}{2} \left[(r_{1G}^2 + r_{2G}^2) \text{cth}(\omega \Delta z) - \frac{2\vec{r}_{1G} \cdot \vec{r}_{2G}}{\sinh(\omega \Delta z)} \right] \right\} \quad (\text{A11})$$

is the solution of Eq. (46) with $\omega = b_0^2/(\nu\alpha_G)$.

Again we can do the replacement $r_{qqi}r_{qqj} \rightarrow r_{qq}^2\delta_{ij}$, perform the derivatives, sum over gluon polarizations, and use Eq. (A6) to obtain

$$\begin{aligned}
 N^G &= m_{N^X B_j} \frac{8\alpha_{em}\alpha_s}{3\pi^4 Q^2} \int d^2 r_{1G} d^2 r_{2G} d\Delta z \\
 &\times \int_{\alpha_G^{\min}}^{\alpha_G^{\max}} \frac{d\alpha_G}{\alpha_G} \sigma_{qq}^N(s, r_{1G}) \sigma_{qq}^N(s, r_{2G}) \frac{b_0^2 e^{Q^2 \Delta z / 2\nu}}{\sinh(\omega \Delta z)} \\
 &\times \left[4 \frac{(\vec{r}_{1G} \cdot \vec{r}_{2G})^2}{r_{1G}^4 r_{2G}^4} + b_0^4 \frac{(\vec{r}_{1G} \cdot \vec{r}_{2G})^2}{r_{1G}^2 r_{2G}^2} + 2b_0^2 \frac{(\vec{r}_{1G} \cdot \vec{r}_{2G})^2}{r_{1G}^2 r_{2G}^4} \right. \\
 &\left. + 2b_0^2 \frac{(\vec{r}_{1G} \cdot \vec{r}_{2G})^2}{r_{1G}^4 r_{2G}^2} - \frac{b_0^2}{r_{1G}^2} - \frac{b_0^2}{r_{2G}^2} - \frac{1}{r_{1G}^2 r_{2G}^2} \right] \\
 &\times \exp[-\beta(r_{1G}^2 + r_{2G}^2) + 2\gamma \vec{r}_{1G} \cdot \vec{r}_{2G}], \quad (\text{A12})
 \end{aligned}$$

where

$$\beta = \frac{b_0^2}{2} [1 + \coth(\omega \Delta z)], \quad (\text{A13})$$

$$\gamma = \frac{b_0^2}{2 \sinh(\omega \Delta z)}. \quad (\text{A14})$$

With a cross section such as $\sigma_{qq}^N(s, r) = C(s)r^2$ the integrations over r_G are easily performed with the result

$$\begin{aligned}
 N^G &= m_{N^X B_j} \frac{8\alpha_{em}\alpha_s C^2(s)}{3\pi^2 Q^2 b_0^2} \int d\Delta z \int_{\alpha_G^{\min}}^{\alpha_G^{\max}} \frac{d\alpha_G}{\alpha_G} \frac{e^{-Q^2 \Delta z / 2\nu}}{\sinh(\omega \Delta z)} \\
 &\times \left\{ \frac{10}{[1 + \coth(\omega \Delta z)]^2} + \frac{12}{\sinh^2(\omega \Delta z) [1 + \coth(\omega \Delta z)]^3} \right. \\
 &\left. - 8 \sinh^2(\omega \Delta z) \ln \left(\frac{1 + \coth(\omega \Delta z)}{2} \right) \right\} \quad (\text{A15})
 \end{aligned}$$

$$\begin{aligned}
 &= \frac{8\alpha_{em}\alpha_s C^2(s)}{3\pi^2 Q^2 b_0^2} \int_0^1 dy \int_{\delta^{\min}}^{\delta^{\max}} \frac{d\delta}{\delta^2} \{ 4y^{1/\delta-2} (1-y^2) \\
 &\times \ln(1-y^2) + 5y^{1/\delta} (1-y^2) + 12y^{1/\delta+2} \}. \quad (\text{A16})
 \end{aligned}$$

In the last step we have introduced the new variables $y = e^{-\omega \Delta z}$ and $\delta = 2b_0^2/(Q^2 \alpha_G)$. According to Eq. (A3) the limits for δ are

$$1 \leq \delta \leq 0.2 \frac{s}{Q^2} - 1. \quad (\text{A17})$$

For the integral containing the logarithm it is convenient to do one more substitution $x = y^2$. Then one finds

$$\begin{aligned}
 &\int_0^1 dy y^{1/\delta-2} (1-y^2) \ln(1-y^2) \\
 &= \frac{1}{2} \lim_{\eta \rightarrow 0} \frac{\partial}{\partial \eta} \int_0^1 dx x^{1/2\delta-3/2} (1-x)^{1+\eta} \quad (\text{A18})
 \end{aligned}$$

$$= \frac{2\delta^2}{\delta^2 - 1} \left[\psi \left(\frac{3}{2} + \frac{1}{2\delta} \right) - \psi(2) \right]. \quad (\text{A19})$$

Now only one integration is left in N^G

$$\begin{aligned}
 N^G &= \frac{64\alpha_{em}\alpha_s C^2(s)}{3\pi^2 Q^2 b_0^2} \int_{\delta^{\min}}^{\delta^{\max}} \frac{d\delta}{\delta} \left\{ \frac{5}{8(1+\delta)} + \frac{7}{8(1+3\delta)} \right. \\
 &\left. - \frac{\delta}{\delta^2 - 1} \left[\psi(2) - \psi \left(\frac{3}{2} + \frac{1}{2\delta} \right) \right] \right\} \quad (\text{A20})
 \end{aligned}$$

and we end up with the result (50) for the factor $\langle P^G \rangle = N^G/D^G$ at $Q^2 \gg b_0^2$.

-
- [1] K. Ackerstaff *et al.*, The HERMES Collaboration, Phys. Lett. B **475**, 386 (2000).
 [2] L.V. Gribov, E.M. Levin, and M.G. Ryskin, Nucl. Phys. **B188**, 555 (1981); Phys. Rep. **100**, 1 (1983).
 [3] A.H. Mueller and J.W. Qiu, Nucl. Phys. **B268**, 427 (1986).
 [4] T.H. Bauer, R.D. Spital, D.R. Yennie, and F.M. Pipkin, Rev. Mod. Phys. **50**, 261 (1978).
 [5] L.L. Frankfurt and M.I. Strikman, Phys. Rep. **160**, 235 (1988).
 [6] B.Z. Kopeliovich, A. Schäfer, and A.B. Tarasov, hep-ph/9908245.
 [7] A.I. B. Zamolodchikov, B.Z. Kopeliovich, and L.I. Lapidus, JETP Lett. **33**, 595 (1981).
 [8] S.J. Brodsky and A. Mueller, Phys. Lett. B **206**, 685 (1988).
 [9] G. Bertsch, S.J. Brodsky, A.S. Goldhaber, and J.F. Gunion, Phys. Rev. Lett. **47**, 297 (1981).
 [10] J.M. Bjorken and J.B. Kogut, Phys. Rev. D **8**, 1341 (1973).
 [11] B.Z. Kopeliovich, J. Raufeisen, and A.V. Tarasov, Phys. Lett. B **440**, 151 (1998).
 [12] J. Raufeisen, A.V. Tarasov, and O. Voskresenskaya, Eur. Phys. J. A **5**, 173 (1999).
 [13] B.G. Zakharov, Phys. At. Nucl. **61**, 838 (1998).
 [14] J.B. Kogut and D.E. Soper, Phys. Rev. D **1**, 2901 (1970).
 [15] J.M. Bjorken, J.B. Kogut, and D.E. Soper, Phys. Rev. D **3**, 1382 (1971).
 [16] N.N. Nikolaev and B.G. Zakharov, Z. Phys. C **49**, 607 (1991).
 [17] K. Golec-Biernat and M. Wüsthoff, Phys. Rev. D **59**, 014017 (1999); **60**, 114023 (1999).

- [18] I.S. Gradshteyn and I.M. Ryzhik, *Table of Integrals, Series, and Products* (Academic, New York, 1994).
- [19] M. Arneodo *et al.*, The NMC Collaboration, Nucl. Phys. **B483**, 3 (1997).
- [20] H. De Vries, C.W. De Jager, and C. De Vries, At. Data Nucl. Data Tables **36**, 469 (1987).
- [21] M. Arneodo *et al.*, The NMC Collaboration, Nucl. Phys. **B481**, 23 (1996).
- [22] V. Barone and M. Genovese, hep-ph/9610206; V. Barone *et al.*, Phys. Lett. B **304**, 176 (1993).
- [23] G.A. Miller, S.J. Brodsky, and M. Karliner, Phys. Lett. B **481**, 245 (2000).